Hindawi Publishing Corporation
Mathematical Problems in Engineering
Volume 2013, Article ID 343851, 9 pages
http://dx.doi.org/10.1155/2013/343851

Research Article

Adaptive Sliding Mode Robust Control for Virtual Compound-Axis Servo System

Yan Ren,[1,2] Zhenghua Liu,[2] Le Chang,[2] and Nuan Wen[2]

[1] *Information Engineering School, Inner Mongolia University of Science and Technology, Baotou 014010, China*
[2] *School of Automation Science and Electrical Engineering, Beihang University, Beijing 100191, China*

Correspondence should be addressed to Yan Ren; renyan.ry@163.com

Received 26 July 2013; Revised 12 October 2013; Accepted 20 October 2013

Academic Editor: Xudong Zhao

A structure mode of virtual compound-axis servo system is proposed to improve the tracking accuracy of the ordinary optoelectric tracking platform. It is based on the structure and principles of compound-axis servo system. A hybrid position control scheme combining the PD controller and feed-forward controller is used in subsystem to track the tracking error of the main system. This paper analyzes the influences of the equivalent disturbance in main system and proposes an adaptive sliding mode robust control method based on the improved disturbance observer. The sliding mode technique helps this disturbance observer to deal with the uncompensated disturbance in high frequency by making use of the rapid switching control value, which is based on the subtle error of disturbance estimation. Besides, the high-frequency chattering is alleviated effectively in this proposal. The effectiveness of the proposal is confirmed by experiments on optoelectric tracking platform.

1. Introduction

Optoelectric tracking (OET) platform is applied to ensure the stability of line of sight (LOS) and achieve the automatic tracking of the maneuvering target under the maneuver motion of carrier and the external disturbance. When the target distance is farther, the small deviation will lead to a large change of the target position. Accordingly, the high tracking accuracy is very important in OET system. The compound-axis system is a form of dual-dimension association control system in the multivariable control systems. It is demonstrated effectively to improve the accuracy and bandwidth of the OET system by inserting a fast steering mirror (FSM) with the high resonant frequency in the large inertia tracking frame of the main optical path [1]. It has been widely applied in high-precision OET systems, satellite laser ranging, laser communications and space remote sensing detection, and so forth [2–5]. But there are some ordinary OET systems without the FSM. Therefore, it is valuable to research how to improve the tracking accuracy of the ordinary OET system.

High-precision motion control is the key of OET device, which directly influences the accuracy of LOS tracking. As a typical kind of servo motor system, the robustness against system uncertainties and external disturbances is urgently required without considering mechanical factors. The disturbance observer (DOB) approach has been widely used as an effective robust method to compensate the disturbance and parameter variations from both environment and system [6, 7]. But DOB only deals with the disturbances in the low-frequency domain. High-frequency components of the disturbances such as sudden changes in external forces and Coulomb friction can degrade the control effect of a DOB based tracking control. Therefore, some researchers have tried to design the fuzzy disturbance observer [8, 9], nonlinear disturbance observer [10, 11] and extended state observer [12, 13].

As one of the most significant approaches, sliding mode control (SMC) has been proven to be an effective robust control strategy for the systems with large uncertainties, nonlinearities, and bounded external disturbances. Consequently, some researchers have actively developed and researched SMC, which is used in uncertain systems [14, 15], time-delay systems [16, 17], fuzzy systems [18, 19], and Markovian jump systems [20, 21]. Besides, a sliding mode disturbance observer (SDOB) was employed in [22]. It can deal with

high-frequency disturbance through selecting appropriate switching control value, which is greater than the upper bound of the disturbance. Meanwhile, the switching control value also causes chattering phenomenon. For alleviating chattering, [23] proposed an SDOB with an adaptive law that requires only a small switching gain. However, this method needs a model of unknown disturbance which is difficult to obtain in engineering practice. As a result, some intelligent methods have been devoted to estimate the upper bound [24, 25]. However, most of these intelligent units are not realized easily in engineering practice, and they are not adequately sensitive to the chattering of control input.

In this paper, the characteristics and structure compound-axis system are analyzed at first. For improving the tracking accuracy of the ordinary OET servo system without the FSM, the design scheme and the realization means of virtual compound-axis are presented. In this method, the adaptive sliding mode controller (ASMC) is designed in main system to reduce the tracking error and deal with high-frequency disturbance by making use of its switching control value, and virtual subsystem employs a hybrid control scheme combining the PD controller (PDC) and feed-forward controller (FFC) simultaneously. The improved DOB compensates disturbance and helps to acquire a small switching gain of ASMC to alleviate the chattering. Experiments are implemented to confirm the validity of this method.

The rest of the paper is organized as follows. Section 2 introduces the OET servo system, including compound-axis system and virtual compound-axis system. Section 3 analyzes the compound control scheme based on virtual compound-axis servo system. Then, the structure and design of DOB based on ASMC are proposed. Experimental results are shown in Section 4. Finally, the conclusion and future work are given in Section 5.

2. OET Servo System

2.1. Compound-Axis OET Servo System. The compound-axis servo system improves the tracking accuracy of optoelectrical tracking system greatly, which is an effective method to lock the beam and target on one point. A typical compound-axis control system uses double detectors structure, including the main-axis system and subaxis system. The main system mainly realizes the coarse tracking and its error is the subsystem input. The subsystem is applied to adjust the tracking residuals of the main system to realize high-precision tracking.

2.2. Virtual Compound-Axis OET Servo System. According to compound-axis control principle, the conception of the virtual compound-axis servo system is put forward in OET system without the FSM. To simplify the problem, this paper analyses a uniaxial platform as an example at first. We assume a coaxial virtual platform that has the same position with the physical platform and a virtual platform owns the virtual tracking detector. Virtual platform connects to the physical platform which connects to foundation bed. The spatial position is overlapped between the tracking detector and virtual tracking detector.

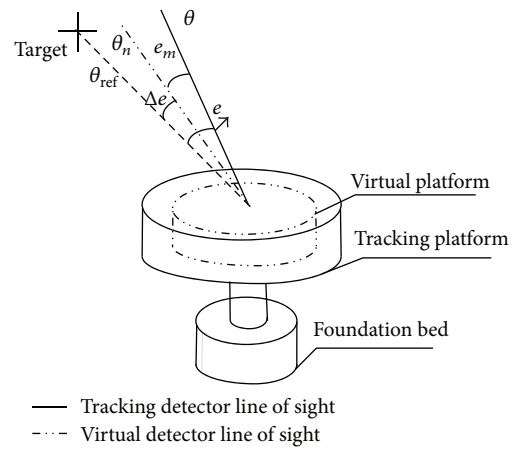

Figure 1: Virtual compound-axis servo system.

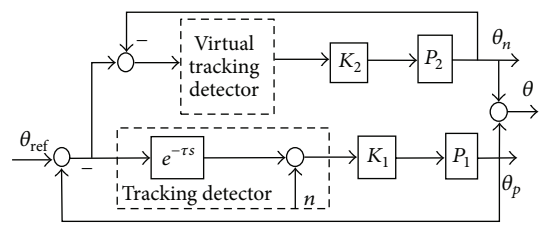

Figure 2: Structure diagram of virtual compound-axis servo system.

The relationship of all the parts of the virtual compound-axis servo system is shown in Figure 1, where e denotes the LOS deviation of the tracking detector and the target, Δe denotes the LOS deviation of the virtual tracking detector and the target, and e_m denotes the LOS deviation of the tracking detector and the virtual tracking detector. The tracking platform tracks the target roughly, while the virtual platform tracks e finely. Therefore, the cooperated tracking mode which is similar to the compound-axis servo system is realized through the combination of main axis and subaxis. The tracking platform is in motion relative to foundation bed and the virtual platform is in motion relative to the tracking platform in motion.

The structure of the virtual compound-axis system is shown in Figure 2, where $K_1(s)$, $K_2(s)$, $P_1(s)$, and $P_2(s)$ denote the tracking loop controller, virtual loop controller, the equivalent characteristic of the tracking platform, and the equivalent characteristic of the virtual platform, respectively. $e^{-\tau s}$ is the tracking detector delay, n is the measuring noise, θ_{ref} is the maneuvering target position in inertia space, θ is the LOS position of the tracking platform, θ_p is the LOS of the tracking detector, and θ_n is the LOS of the virtual tracking detector.

The delay factor only affects the phase-frequency characteristic of the system but does not affect the gain of the system. In order to simplify the analysis, the delay factor and the transfer function of the virtual tracking detector are

ignored. Then, the closed-loop transfer function of the system is expressed as

$$G(s) = \frac{K_1(s)P_1(s) + K_2(s)P_2(s) + K_1(s)P_1(s)K_2(s)P_2(s)}{[1 + K_1(s)P_1(s)][1 + K_2(s)P_2(s)]}. \quad (1)$$

The transfer functions of main system and subsystem are described as follows, respectively:

$$G_1(s) = \frac{K_1(s)P_1(s)}{1 + K_1(s)P_1(s)}, \qquad G_2(s) = \frac{K_2(s)P_2(s)}{1 + K_2(s)P_2(s)}. \quad (2)$$

From (1)-(2), the poles of the entire system are the poles of the main system and subsystem. Only if the main system and subsystem are stable, the entire system is stable.

Suppose $e_1(s)$ as the error of the main system and $e_2(s)$ as the error of the subsystem. The error of subsystem can be obtained as

$$e_2(s) = \frac{e_1(s)}{1 + K_2(s)P_2(s)} = \frac{\theta_{\text{ref}}(s)}{[1 + K_1(s)P_1(s)][1 + K_2(s)P_2(s)]}. \quad (3)$$

From (3), the tracking accuracy of the virtual compound-axis system can be improved by controlling the main system and subsystem. And the error of the system is the error of subsystem. Therefore, the virtual compound-axis system owns the high tracking accuracy.

2.3. Virtual Compound-Axis Servo System Implementation. Two problems should be solved as virtual compound-axis servo system:

(1) problem of virtual objects property, namely how to determine the transfer function of the virtual platform;

(2) problem of implementing the virtual compound-axis servo system, namely, how to achieve the coarse-fine tracking mode on a single tracking platform.

In order to implement virtual compound-axis servo system, its control structure diagram is shown in Figure 3, where the delay of the tracking detector and virtual detector is ignored. In Figure 3, main system is tracking platform, subsystem is virtual tracking platform, and e is the input signal of the subsystem. In order to simplify the design, the transfer function of virtual platform uses the nominal model of the practical system. As the tracking accuracy of virtual platform is better than that of the tracking platform, the tracking platform tracks virtual platform to decrease e_m for getting high tracking accuracy. In Figure 3, K_1 and K_2 are the position controllers of the main system and subsystem.

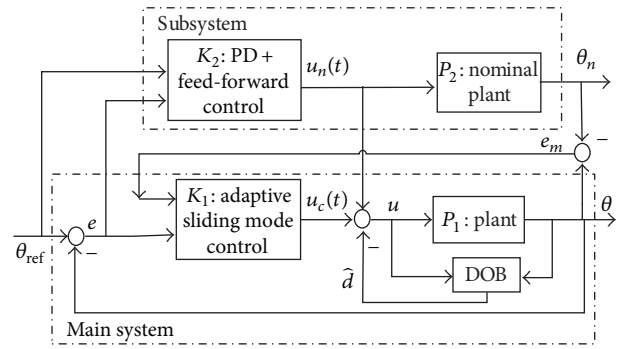

Figure 3: Control realization diagram of virtual compound-axis servo system.

In order to get the satisfactory control effect, the ASMC is used in the main system and PDC and FFC are adopted in the system. The output of PDC and FFC which can be regarded as a control component of the main system provides control variable to the actual plant.

3. Compound Control Scheme of Virtual Compound-Axis Servo System

3.1. Controller Design of Subsystem. Because a LOS stabilization servo system is driven by a DC torque motor, the dynamics of the plant can be described as

$$J\ddot{\theta} + B\dot{\theta} = u + f(\cdot), \quad (4)$$

where J, B, θ, and u denote the inertia mass, the damping, the angular position response, and the control input, respectively. $f(\cdot)$ denotes the disturbance such as nonlinear friction, the force from the environment, the carrier disturbance, and unknown, time-varying, and nonlinear dynamics, which is difficult to model. Consider that $J_m \le J \le J_M$, $B_m \le B \le B_M$ is satisfied, where J_m, J_M, B_m, and B_M are positive real number.

By assembling the parameter mismatch, external disturbance, and unknown dynamics into an equivalent disturbance d, (4) can be written as

$$J_n\ddot{\theta} + B_n\dot{\theta} = u + d, \quad (5)$$

where J_n and B_n denote the nominal mass and the nominal damping, respectively. The equivalent disturbance is given by $d = (J_n - J)\ddot{\theta} + (B_n - B)\dot{\theta} + f(\cdot)$.

Define a tracking error of the system as $e = \theta_{\text{ref}} - \theta$, where θ_{ref} is a given reference signal. Using the structure of virtual compound-axis for system (5), the control value u can be described as

$$u = u_n + u_c - \hat{d}, \quad (6)$$

where u_n and u_c are the control value of subsystem and main system, respectively. $\hat{d}$ is the estimated disturbance through DOB. When the equivalent disturbance and parameters meet requirements, the task is to design u_c and u_n to make $e \to 0$.

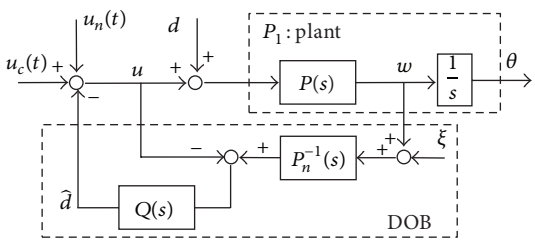

Figure 4: Basic diagram of DOB.

The subsystem nominal model is described as follows:

$$J_n\ddot{\theta} + B_n\dot{\theta} = u_n. \tag{7}$$

The controller of subsystem uses a hybrid control scheme combining PDC and FFC, which can be described as

$$\begin{aligned} u_{PD} &= k_P e + k_D \dot{e}, \\ u_{\mathrm{FFC}} &= J_n\ddot{\theta}_{\mathrm{ref}} + B_n\dot{\theta}_{\mathrm{ref}}, \end{aligned} \tag{8}$$

where k_P and k_D denote proportional coefficient and differential coefficient, respectively.

An approximate method for difference to estimate the reference values of velocity and acceleration is introduced. This method is expressed by [26]

$$\begin{aligned} \dot{\hat{\theta}}_{\mathrm{ref}} &= \frac{gs}{s+g}\theta_{\mathrm{ref}}, \\ \ddot{\hat{\theta}}_{\mathrm{ref}} &= \left(\frac{gs}{s+g}\right)^2\theta_{\mathrm{ref}} = \frac{gs}{s+g}\dot{\hat{\theta}}_{\mathrm{ref}}, \end{aligned} \tag{9}$$

where s is used to concatenate one low-pass filter, whose cut-off frequency is $g > 0$.

Thence, the output of controller is written as (8):

$$u_n = u_{PD} + u_{\mathrm{FFC}} = k_P e + k_D\dot{e} + J_n\ddot{\hat{\theta}}_{\mathrm{ref}} + B_n\dot{\hat{\theta}}_{\mathrm{ref}}. \tag{10}$$

3.2. Disturbance Observer-Based Main System Control. In the OET system, nonlinear dynamic and uncertain elements are difficult to compensate by accurate model. Robust closed-loop control method based on DOB, which is widely applied in the high-precision servo system, has simple design process. It can inhibit the variety of external disturbances and parameters effectively.

In order to realize disturbances suppression, the equal compensation is introduced into control input by means of the estimation of the DOB improved in this paper. The basic idea of DOB is shown in Figure 4. In Figure 4, $P(s)$, $P_n(s)$, and $Q(s)$ represent the velocity model of the actual plant, the nominal velocity model, a filter, respectively. s means Laplace operator. w, ξ, and $\hat{d}$ are the actual velocity output, the measurement noise, and the estimated disturbances, respectively. Let u, d and ξ be system input. The velocity response can be acquired on the basis of superposition principle:

$$w(s) = G_{UW}(s)\,u(s) + G_{DW}(s)\,d(s) + G_{\xi W}(s)\,\xi(s), \tag{11}$$

where

$$\begin{aligned} G_{UW}(s) &= \frac{P(s)\,P_n(s)}{P_n(s) + [P(s) - P_n(s)]\,Q(s)}, \\ G_{DW}(s) &= \frac{P(s)\,P_n(s)\,[1 - Q(s)]}{P_n(s) + [P(s) - P_n(s)]\,Q(s)}, \\ G_{\xi W}(s) &= \frac{P(s)\,Q(s)}{P_n(s) + [P(s) - P_n(s)]\,Q(s)}. \end{aligned} \tag{12}$$

Assume that the bandwidth of ideal filter $Q(s)$ is f_0. At low frequencies, there is $Q(s) \approx 1$ when frequency $f \le f_0$; therefore $G_{UW}(s) \approx P_n(s)$, $G_{DW}(s) \approx 0$ and $G_{\xi W}(s) \approx 1$. This means that DOB makes the characteristic of the actual plant approximately the same as that of the nominal model in low-frequency domain. Therefore, the system has powerful inhibiting effect against external disturbances. DOB is very sensitive to low-frequency noise. In practical applications, it is necessary to consider that appropriate measures are taken to reduce the low-frequency noise in the measurement of the motion state.

In high-frequency domain, if frequency $f > f_0$, then $Q(s) \approx 0$. Consequently $G_{UW}(s) = G_{DW}(s) = P(s)$ and $G_{\xi W}(s) = 0$. This means that DOB has no inhibiting effects on external disturbances while having great inhibiting ability against the high-frequency measurement noise.

The simplified nominal velocity model is procured as follows:

$$P_n(s) = \frac{1}{J_n s + B_n}. \tag{13}$$

$Q(s)$ design is significant in DOB design. The design method of low-pass filter $Q(s)$ was proposed [27]. The relative degree of $Q(s)$ must be equal to or greater than that of $P_n^{-1}(s)$, in order to make $Q(s)P_n^{-1}(s)$ regular. According to the nominal model shown in (13), the following is chosen for this research, which satisfies the property stated above:

$$Q(s) = \frac{g}{s+g}, \tag{14}$$

where g is the cut-off frequency of the low-pass filter (LPF) in DOB. Then, the estimated disturbance is described as

$$\hat{d} = Q(s)\,d = \frac{g}{s+g}d. \tag{15}$$

Taking into account the physical realization of $J_n s$, $\hat{d}$ is represented as follows:

$$\begin{aligned} \hat{d} &= Q(s)\left[(J_n s + B_n)\,w - u\right] \\ &= \frac{g}{s+g}\left[(J_n s + B_n)\,w - u\right] \\ &= J_n g w - \frac{g}{s+g}\left[(J_n g - J_n B_n)\,w + u\right]. \end{aligned} \tag{16}$$

Therefore, the improved DOB can be obtained as shown in Figure 5. The improved DOB has only one differential element, simple structure, and small calculation.

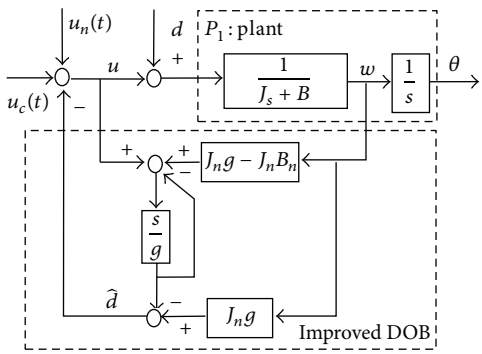

Figure 5: Structural diagram of improved DOB.

The nonlinear function $f(\cdot)$ can be modeled by the improved DOB system as

$$f(\cdot) = \hat{d} + \delta, \tag{17}$$

where δ is the approximation error of the DOB. Considering δ is a bounded variable, φ is defined to meet

$$|\delta| < \varphi, \tag{18}$$

where $\varphi > 0$, $\tilde{\varphi} = \varphi - \hat{\varphi}$, and $\dot{\tilde{\varphi}} = -\dot{\hat{\varphi}}$. $\hat{\varphi}$ are introduced to assist in estimating the switching gain of the sliding mode controller which is designed in Section 3.3.

3.3. Adaptive Sliding Mode Controller Based Main System Design. Define the tracking error of model as $e_m = \theta - \theta_n$, where θ_n is an output value of subsystem. Define a sliding mode z as follows:

$$z = \dot{e}_m + \lambda e_m, \quad \lambda = \frac{B_n}{J_n}. \tag{19}$$

Then, u_c is designed as

$$u_c = -Kz - h \cdot \operatorname{sgn}(z) - \frac{J_n - \hat{J}}{J_n} u_n + \hat{B}\dot{\theta} - \lambda \hat{J}\dot{\theta}, \tag{20}$$

where K is a positive constant gain and h is a positive switching gain. $\hat{J}$ and $\hat{B}$ are the estimation values of J and B, respectively. $\operatorname{sgn}(z)$ is a sign function that is defined as follows:

$$\operatorname{sgn}(z) = \begin{cases} 1, & z > 0, \\ 0, & z = 0, \\ -1, & z < 0. \end{cases} \tag{21}$$

The adaptive law is adopted:

$$\begin{aligned} \dot{\hat{J}} &= \operatorname{Proj}_J\left(-r_1\left(\frac{1}{J_n}u_n - \lambda\dot{\theta}\right)z\right), \\ \dot{\hat{B}} &= \operatorname{Proj}_B\left(-r_2\dot{\theta}z\right), \\ \dot{\hat{\varphi}} &= \operatorname{Proj}_\varphi\left[r_3 z \operatorname{sgn}(z)\right], \\ h &= \hat{\varphi}, \end{aligned} \tag{22}$$

where r_1, r_2, and r_3 are positive real constants. The function $\operatorname{Proj}_\bullet(v)$ is defined as

$$\operatorname{Proj}_\bullet(v) = \begin{cases} v, & \bullet_m < \hat{\bullet} < \bullet_M \\ 0, & \hat{\bullet} = \bullet_M \text{ and } v > 0 \\ 0, & \hat{\bullet} = \bullet_m \text{ and } v < 0, \end{cases} \tag{23}$$

where $\bullet_m$ is the minimum value of $\hat{\bullet}$ and $\bullet_M$ is the maximum value of $\hat{\bullet}$.

Theorem 1. *For system* (4), *if the condition* $|\delta| < \varphi$ *is satisfied,* z *exponentially decays to zero, and* e_m *asymptotically decays to zero using the control law as* (10), (15), (20), *and* (22). *The state variables of the system are bounded meanwhile.*

Proof. Define a positive-definite Lyapunov candidate:

$$V(z) = \frac{1}{2}Jz^2 + \frac{1}{2r_1}\tilde{J}^2 + \frac{1}{2r_2}\tilde{B}^2 + \frac{1}{2r_3}\tilde{\varphi}^2, \tag{24}$$

$$\begin{aligned} J\dot{z} &= J\left[\left(\ddot{\theta} - \ddot{\theta}_n\right) + \lambda\left(\dot{\theta} - \dot{\theta}_n\right)\right] \\ &= \left(J\ddot{\theta} + B\dot{\theta}\right) - \frac{J}{J_n}\left(J_n\ddot{\theta}_n + B_n\dot{\theta}_n\right) - B\dot{\theta} + \lambda J\dot{\theta} \\ &= u_c + f(\cdot) - \hat{d} + u_n - \frac{J}{J_n}u_n - B\dot{\theta} + \lambda J\dot{\theta} \\ &= u_c + \delta + \frac{J_n - J}{J_n}u_n - B\dot{\theta} + \lambda J\dot{\theta}. \end{aligned} \tag{25}$$

Define $\tilde{J} = J - \hat{J}$, $\tilde{B} = B - \hat{B}$; then $\dot{\tilde{J}} = -\dot{\hat{J}}$, $\dot{\tilde{B}} = -\dot{\hat{B}}$.

Substitute (20) into (25):

$$\begin{aligned} J\dot{z} &= -Kz - h \cdot \operatorname{sgn}(z) - \frac{J_n - \hat{J}}{J_n}u_n \\ &\quad + \hat{B}\dot{\theta} - \lambda\hat{J}\dot{\theta} + \frac{J_n - J}{J_n}u_n - B\dot{\theta} + \lambda J\dot{\theta} + \delta \\ &= -Kz - h \cdot \operatorname{sgn}(z) + \left(\hat{J} - J\right)\left(\frac{1}{J_n}u_n - \lambda\dot{\theta}\right) \\ &\quad + \left(\hat{B} - B\right)\dot{\theta} + \delta \\ &= -Kz - h \cdot \operatorname{sgn}(z) - \tilde{J}\left(\frac{1}{J_n}u_n - \lambda\dot{\theta}\right) - \tilde{B}\dot{\theta} + \delta \\ \dot{V}(z) &= -Kz^2 - h \cdot z \operatorname{sgn}(z) - \tilde{J}z\left(\frac{1}{J_n}u_n - \lambda\dot{\theta}\right) \\ &\quad - \tilde{B}z\dot{\theta} - \frac{1}{r_1}\tilde{J}\dot{\hat{J}} - \frac{1}{r_2}\tilde{B}\dot{\hat{B}} - \frac{1}{r_3}\tilde{\varphi}\dot{\hat{\varphi}} + z\delta \\ &= -Kz^2 - h \cdot z \operatorname{sgn}(z) - \tilde{J}\left[z\left(\frac{1}{J_n}u_n - \lambda\dot{\theta}\right) + \frac{1}{r_1}\dot{\hat{J}}\right] \\ &\quad - \tilde{B}\left(z\dot{\theta} + \frac{1}{r_2}\dot{\hat{B}}\right) - \frac{1}{r_3}\tilde{\varphi}\dot{\hat{\varphi}} + z\delta. \end{aligned} \tag{26}$$

According to (22), the time derivative of Lyapunov function becomes

$$\begin{aligned}\dot{V}(z) &= -Kz^2 - \widehat{\varphi}\cdot z\,\mathrm{sgn}(z) - |z|\,\widetilde{\varphi} + z\delta \\ &\le -Kz^2 - \varphi|z| + |z|\,|\delta| \\ &= -Kz^2 - |z|\left(\varphi - |\delta|\right).\end{aligned} \tag{27}$$

Since $|\delta| < \varphi$, then $|z|(\varphi - |\delta|) > 0$. Therefore, $\dot{V}(z) \le -kz^2$ is met.

According to (24), there is

$$z^2(t) \le z(0)^2 \exp\left(-\frac{K}{J}t\right), \tag{28}$$

which implies that z exponentially decays to zero. Then, according to the definition of $z = \dot{e}_m + \lambda e_m$, e_m asymptotically decays to zero. If $e_m(0)$ and $\dot{e}_m(0)$ are bounded, then $e_m(t)$ and $\dot{e}_m(t)$ are bounded to arbitrary $t > 0$ because of $z(t)$ being uniformly bounded. If $\theta_n(0)$ and $\dot{\theta}_n(0)$ are bounded, then $\theta_n(t)$ and $\dot{\theta}_n(t)$ are bounded. According to $e_m = \theta - \theta_n$, θ and $\dot{\theta}$ are bounded. Consequently, the state variables of the system are bounded.

Theorem 1 is proved. □

In this method, the switching gain h is only required to be greater than $|\delta|$, which is a small variable. This design alleviates the chattering phenomenon of sliding mode controller. In engineering practice, since sign function sgn(·) in control law (20) can cause the frequent switching of the control variable and result in the output chattering, it is easy to damage the power amplifier. In order to avoid frequent switching of the control output, the sgn(·) is replaced by the saturation function (29) to weaken the chattering further:

$$\mathrm{sat}\left(\frac{x}{\Delta}\right) = \begin{cases} 1, & x > \Delta, \\ \dfrac{1}{\Delta}x, & |x| \le \Delta, \\ -1, & x < -\Delta, \end{cases} \tag{29}$$

where Δ is positive real constant, namely, the width of a boundary layer.

Introducing sat(·), control law (20) becomes

$$u_c = -Kz - h\cdot\mathrm{sat}\left(\frac{hz}{4\varepsilon}\right) - \frac{J_n - \widehat{J}}{J_n}u_n + \widehat{B}\dot{\theta} - \lambda\widehat{J}\dot{\theta}, \tag{30}$$

where ε is a small positive constant. Then, there is the following Theorem 2.

Theorem 2. *For system* (4)*, if the condition* $|\delta| < \varphi$ *is satisfied and the control law as* (10), (15), (22), *and* (30) *is adopted, then*

(1) z *exponentially decays to zero, and* $\lim_{t\to\infty}|z(t)| \le \sqrt{\varepsilon/K}$ *is met;*

(2) e_m *asymptotically decays to zero, and* $\lim_{t\to\infty}|e_m(t)| \le (1/\lambda)\sqrt{\varepsilon/K}$ *is met;*

(3) $\dot{e}_m(t)$ *asymptotically converges, and* $\lim_{t\to\infty}|\dot{e}_m(t)| \le 2\sqrt{\varepsilon/K}$ *is met.*

Proof. Select the positive-definite function $V(z)$ as (24); then its time derivative is calculated as

$$\begin{aligned}\dot{V}(z) &= -Kz^2 - h\cdot z\,\mathrm{sat}\left(\frac{hz}{4\varepsilon}\right) - \widetilde{J}z\left(\frac{1}{J_n}u_n - \lambda\dot{\theta}\right) \\ &\quad - \widetilde{B}z\dot{\theta} - \frac{1}{r_1}\widetilde{J}\dot{\widehat{J}} - \frac{1}{r_2}\widetilde{B}\dot{\widehat{B}} - \frac{1}{r_3}\widetilde{\varphi}\dot{\widehat{\varphi}} + z\delta \\ &= -Kz^2 - h\cdot z\,\mathrm{sat}\left(\frac{hz}{4\varepsilon}\right) - \widetilde{J}\left[z\left(\frac{1}{J_n}u_n - \lambda\dot{\theta}\right) + \frac{1}{r_1}\dot{\widehat{J}}\right] \\ &\quad - \widetilde{B}\left(z\dot{\theta} + \frac{1}{r_2}\dot{\widehat{B}}\right) - \frac{1}{r_3}\widetilde{\varphi}\dot{\widehat{\varphi}} + z\delta \\ &= -Kz^2 - \widehat{\varphi}z\,\mathrm{sat}\left(\frac{hz}{4\varepsilon}\right) - \widetilde{\varphi}z\,\mathrm{sat}\left(\frac{hz}{4\varepsilon}\right) + |z|\,\delta \\ &= -Kz^2 - \varphi z\,\mathrm{sat}\left(\frac{hz}{4\varepsilon}\right) + |z|\,\delta.\end{aligned} \tag{31}$$

Since $|z| \ge 4\varepsilon/h$, $\mathrm{sat}(hz/4\varepsilon) = \mathrm{sgn}(z)$. According to the proof of Theorem 1, when $\varphi \ge |\delta|$, $\dot{V}(z) \le -kz^2$ is met. Therefore, z exponentially converges until

$$\lim_{t\to\infty}|z(t)| < \frac{4\varepsilon}{h}. \tag{32}$$

If $|z| < 4\varepsilon/h$, then $\mathrm{sat}(hz/4\varepsilon) = hz/4\varepsilon$. $\dot{V}(z)$ is described as

$$\begin{aligned}\dot{V}(z) &\le -Kz^2 - \varphi\frac{h|z|^2}{4\varepsilon} + |z|\,|\delta| \\ &\le -Kz^2 - \frac{\varphi^2|z|^2}{4\varepsilon} + \varphi|z| \\ &\le -Kz^2 - \frac{1}{\varepsilon}\left(\frac{1}{2}\varphi|z| - \varepsilon\right)^2 + \varepsilon \\ &\le -Kz^2 + \varepsilon \le -\frac{2K}{J}V + \varepsilon.\end{aligned} \tag{33}$$

Consequently,

$$V(t) \le \exp^{-(2K/J)t}V(0) + \frac{J\varepsilon}{2K}\left(1 - \exp^{-(2K/J)t}\right). \tag{34}$$

From (34), yield to

$$\lim_{t\to\infty}|z(t)| \le \sqrt{\frac{\varepsilon}{K}}. \tag{35}$$

It is similar to Theorem 1 that the state variables are bounded in this system. From (35), z asymptotically converges to the bounded region. According to (19), $e_m(t)$ and $\dot{e}_m(t)$ are satisfied as follows:

$$\begin{aligned}\lim_{t\to\infty}\left|e_m(t)\right| &\le \frac{1}{\lambda}\sqrt{\frac{\varepsilon}{K}}, \\ \lim_{t\to\infty}\left|\dot{e}_m(t)\right| &\le 2\sqrt{\frac{\varepsilon}{K}},\end{aligned} \tag{36}$$

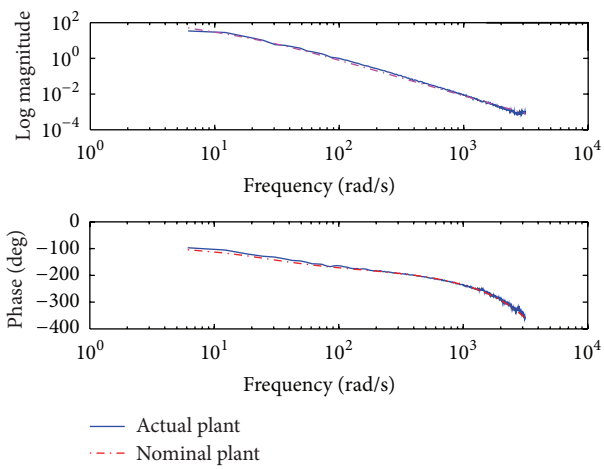

Figure 6: Fitting curves for frequency characteristics of actual plant and nominal model.

which means that $e_m(t)$ and $\dot{e}_m(t)$ asymptotically converge to the bounded region.

Theorem 2 is proved. □

4. Experiment Results

This section investigates the feasibility and effectiveness of the proposed compound controller based on the structure of the virtual compound-axis servo system by experiments. The tracking experiments are implemented through using some type of OET platform. The position sensor of the device uses the optical-electrical encoder with resolution of 0.0007 degrees. The control algorithm program is written with C language based on Windows-RTX real-time system in an industrial computer, which adopts Advantech IPC 610 and connects with the servo drivers by a 16-bit D/A convertor of PCI bus. The control cycle is 0.001 s. It is worth mentioning that the adaptive online adjustment will consume lots of computational resource. With the development of the advanced technologies on computer, the problem of lots of computation has been solved. The proposed adaptive sliding controller is proved to be feasible in a practical system by this experimental platform.

Based on what has been mentioned above, the pitch axis is chosen herein to verify the method because each axis of the OET platform can be designed independently. The parameters of the nominal model are identified as $J_n = 0.000125\,\text{kg}$ and $B_n = 0.003125\,\text{N}\cdot\text{s}\cdot\text{m}^{-1}$ by a white noise frequency sweep method. The fitting curves for frequency characteristics of actual plant and nominal model are shown in Figure 6.

The experiments are separated into two parts. First, the experiment is completed under the proposed compound control scheme, in which sign function uses saturation function. Second, in order to verify the effect of the proposed method, a comparative experiment is achieved by the traditional control scheme with PDC + FFC + DOB. Other parameters are given as follows: $k_P = 0.45$, $k_D = 0.12$, $K = 0.04$, $r_1 = 0.01$, $r_2 = 0.001$, $r_3 = 0.005$, and $\varepsilon = 0.0002$. Considering the modeling mismatch and the robustness of the system, the value of parameter g in improved DOB is chosen as 1000 rad/s.

Figure 7 compares the tracking error and the control value of the two control schemes when the reference input signal is a sinusoidal signal where the amplitude is 2 degrees and frequency is 0.5 Hz. The results indicate that the proposed control scheme could achieve a better position tracking performance than traditional control laws: a maximum tracking error decreases from 0.052 degrees to 0.023 degrees with the help of the ASMC. ASMC achieves the adjustment to e_m better. From Figure 7(a), we can see that the tracking error reaches the maximum value at zero velocity, and the tracking error of the proposed control scheme is smaller. Compared with traditional control scheme, the compound control scheme based on the virtual compound-axis system has better tracking performance and robustness. The disturbance is sufficiently compensated by using improved DOB, which simplifies design process and decreases calculation time. Meanwhile, the accuracy of the system is guaranteed by introducing ASMC to adjust e_m again, whose gain is greatly related to the upper bound on the error of the disturbance estimation, and the reduction of switching gain helps to alleviate the chattering. Figure 7(b) illustrates that the controller output curve of the compound control scheme is smoother than that of traditional control scheme.

In order to test the dynamic performance of the tracking object further, the tracking command signal is employed as $\sin(2\pi \cdot 3t)$. Figure 8(a) shows that the maximum tracking error decreases from 0.14 degrees to 0.06 degrees under the reference signal. Compared to the traditional control scheme, the system with compound control scheme has better dynamic performance. The testing standard of OET platform stipulates that the maximum tracking error cannot exceed 10% of the amplitude of the reference signal in working band. Obviously, the tracking errors of Figures 7(a) and 8(a) meet this standard under the proposed method. Because it has a switching control, the adaptive sliding mode technique can reject the impact of nonlinear disturbance in high-frequency domain which is not compensated by the DOB. From this point of view, the proposed control scheme enhances the system robustness. Furthermore, according to Figures 7(b) and 8(b), the control value of the proposed method is far less than the limit of the D/A converter. The control value does not exhibit obvious chattering phenomenon because ASMC with the improved DOB can alleviate the chattering phenomenon. Consequently, the proposed scheme not only ensures strong robustness against system uncertainties and small tracking error but also suppresses the high-frequency chattering at control input effectively. The results indicate that the compound controller can be reliably performed in practical application.

5. Conclusions

To obtain the high performance and good robustness for ordinary OET system without the FSM, the design method of virtual compound-axis servo system is proposed in this paper. The proposed compound control scheme based on the

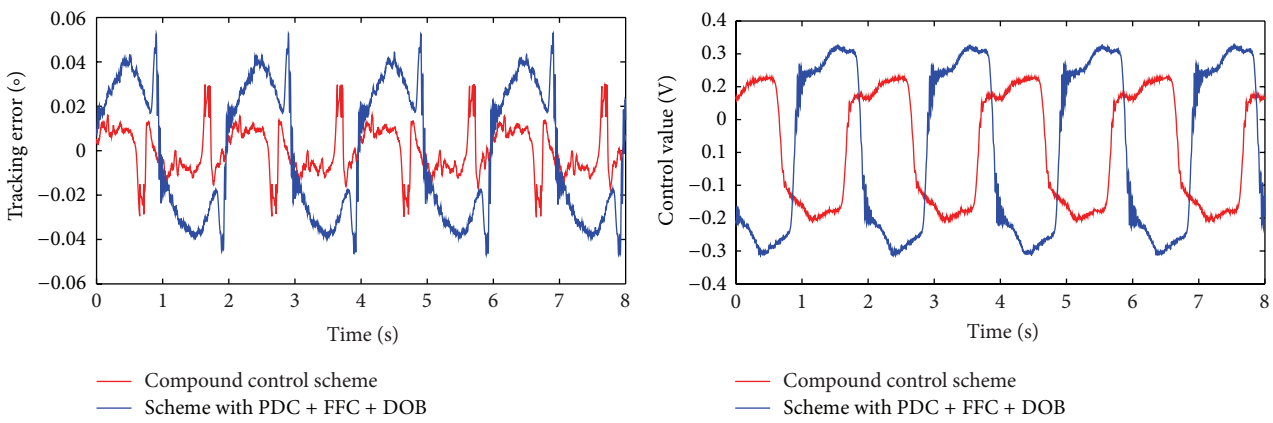

(a) Comparison of tracking error curves (b) Comparison of control value

FIGURE 7: Comparison curves under two schemes with sinusoidal input ($A = 2^\circ$, $f = 0.5$ Hz).

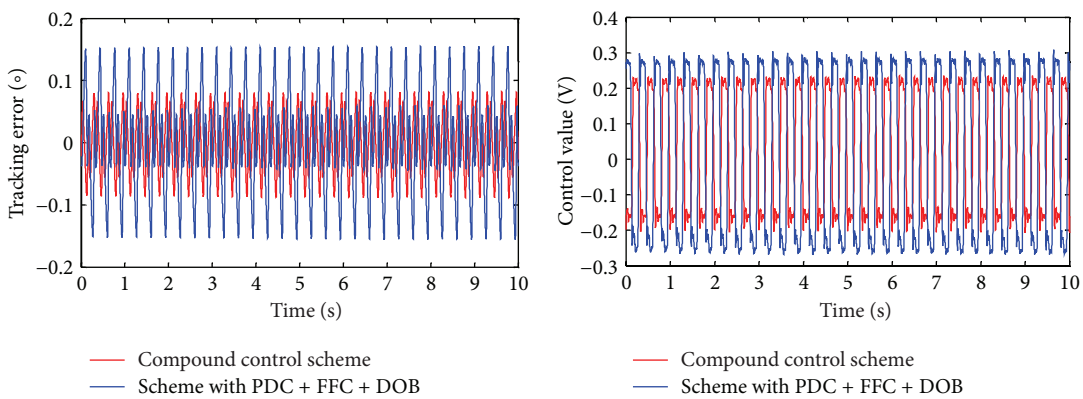

(a) Comparison of tracking error curves (b) Comparison of control value

FIGURE 8: Comparison curves under two schemes with sinusoidal input ($A = 1^\circ$, $f = 3$ Hz).

structure of the virtual compound-axis system can maintain the robustness of OET system against various disturbances in the whole control period, and then the tracking error of OET system can be limited within an expected level in the existence of sustained uncertainties. Although the virtual compound-axis does not perform as well as the real compound-axis, it can also improve the tracking precision of the OET system to some extent. Therefore, the proposed method can be used as a new control technology applied in OET system. In addition, because OET system is a typical servo motion system, the theoretic results are able to be extended to other relational fields.

However, the velocity and acceleration command signal in FFC cannot be measured directly and easily in practice. Therefore, some more excellent differential methods should be considered in further work. Simultaneously, in order to track the maneuvering target with higher speed, further studies aimed at better performance at higher frequencies are needed. Besides, with the development of advanced computer and information technologies, massive amount of measurement data can be utilized to extract the useful information about the current state of the OET process. As a result, the excellent method of the process monitoring and fault diagnosis, such as data-driven techniques [28], can be used as references in future work.

Conflict of Interests

The authors declare that there is no conflict of interests regarding the publication of this paper.

Acknowledgments

This work was supported by the National Basic Research Program (Grant no. 2012CB821200) and the Scientific Research for Colleges and Universities of Inner Mongolia (Grant no. NJZY13143) in China.

References

[1] W. Thanmas, "Digital laser ranging and tracking using a compound axis servomechanism," *Applied Optics*, vol. 5, no. 4, pp. 497–505, 1966.

[2] J. M. Hilkert, "Inertially stabilized platform technology concepts and principles," *IEEE Control Systems Magazine*, vol. 28, no. 1, pp. 26–46, 2008.

[3] Y. Song, "Variable structure control technology of the fine tracking assembly in airborne laser communication system," *Infrared and Laser Engineering*, vol. 39, no. 5, pp. 934–938, 2010 (Chinese).

[4] M. Guelman, A. Kogan, A. Kazarian, A. Livne, M. Orenstein, and H. Michalik, "Acquisition and pointing control for inter-satellite laser communications," *IEEE Transactions on Aerospace and Electronic Systems*, vol. 40, no. 4, pp. 1239–1248, 2004.

[5] Q. Wang, "Single detector compound axis control based on real-time predicted trajectory correcting method," *Opto-Electronic Engineering*, vol. 34, no. 4, pp. 17–21, 2007.

[6] T. R. Grochmal and A. F. Lynch, "Precision tracking of a rotating shaft with magnetic bearings by nonlinear decoupled disturbance observers," *IEEE Transactions on Control Systems Technology*, vol. 15, no. 6, pp. 1112–1121, 2007.

[7] K. Kyung-Soo, R. Keun-Ho, and K. Soohyun, "Disturbance observer for estimating higher order disturbances in time series expansion," *IEEE Transactions on Automatic Control*, vol. 55, no. 8, pp. 1905–1911, 2010.

[8] E. Kim, "A fuzzy disturbance observer and its application to control," *IEEE Transactions on Fuzzy Systems*, vol. 10, no. 1, pp. 77–84, 2002.

[9] Y. Wu, Y. Liu, and D. Tian, "A compound fuzzy disturbance observer based on sliding modes and its applicaton on flight simulator," *Mathematical Problems in Engineering*, vol. 2013, Article ID 913538, 8 pages, 2013.

[10] F.-J. Lin, P.-H. Chou, and Y.-S. Kung, "Robust fuzzy neural network controller with nonlinear disturbance observer for two-axis motion control system," *IET Control Theory and Applications*, vol. 2, no. 2, pp. 151–167, 2008.

[11] X. Chen, C.-Y. Su, and T. Fukuda, "A nonlinear disturbance observer for multivariable systems and its application to magnetic bearing systems," *IEEE Transactions on Control Systems Technology*, vol. 12, no. 4, pp. 569–577, 2004.

[12] S. Li, J. Yang, W.-H. Chen, and X. Chen, "Generalized extended state observer based control for systems with mismatched uncertainties," *IEEE Transactions on Industrial Electronics*, vol. 59, no. 12, pp. 4792–4802, 2012.

[13] B.-Z. Guo and Z.-L. Zhao, "On convergence of non-linear extended state observer for multi-input multi-output systems with uncertainty," *IET Control Theory & Applications*, vol. 6, no. 15, pp. 2375–2386, 2012.

[14] Q. Khan, A. I. Bhatti, M. Iqbal, and Q. Ahmed, "Dynamic integral sliding mode control for SISO uncertain nonlinear systems," *International Journal of Innovative Computing, Information and Control*, vol. 8, no. 7, pp. 4621–4633, 2012.

[15] T. H. Yan, B. He, X. D. Chen, and X. S. Xu, "The discrete-time sliding mode control with computation time delay for repeatable run-out compensation of hard disk drives," *Mathematical Problems in Engineering*, vol. 2013, Article ID 505846, 13 pages, 2013.

[16] L. Wu and W. X. Zheng, "Passivity-based sliding mode control of uncertain singular time-delay systems," *Automatica*, vol. 45, no. 9, pp. 2120–2127, 2009.

[17] Y. Niu, J. Lam, X. Wang, and D. W. C. Ho, "Observer-based sliding mode control for nonlinear state-delayed systems," *International Journal of Systems Science*, vol. 35, no. 2, pp. 139–150, 2004.

[18] N. Yagiz, Y. Hacioglu, and Y. Taskin, "Fuzzy sliding-mode control of active suspensions," *IEEE Transactions on Industrial Electronics*, vol. 55, no. 11, pp. 3883–3890, 2008.

[19] J. H. Zhang, P. Shi, and Y. Q. Xia, "Robust adaptive sliding-mode control for fuzzy systems with mismatched uncertainties," *IEEE Transactions on Fuzzy Systems*, vol. 18, no. 4, pp. 700–711, 2010.

[20] Y. Niu, D. W. C. Ho, and X. Wang, "Sliding mode control for Itô stochastic systems with Markovian switching," *Automatica*, vol. 43, no. 10, pp. 1784–1790, 2007.

[21] L. Wu, W. X. Zheng, and H. Gao, "Dissipativity-based sliding mode control of switched stochastic systems," *IEEE Transactions on Automatic Control*, vol. 58, no. 3, pp. 785–791, 2012.

[22] R. Yan, L. Zhenghua, and Z. Rui, "Application of low speed opto-electronic tracking systems based on sliding mode distutbance observer," *Journal of Beihang University of Aeronautics and Astronautics*, vol. 39, no. 6, pp. 835–840, 2013 (Chinese).

[23] Y. Lu, "Sliding-mode disturbance observer with switching-gain adaptation and its application to optical disk drives," *IEEE Transactions on Industrial Electronics*, vol. 56, no. 9, pp. 3743–3750, 2009.

[24] M. Zhihong, X. H. Yu, K. Eshraghian, and M. Palaniswami, "A robust adaptive sliding mode tracking control using an RBF neural network for robotic manipulators," in *Proceedings of the IEEE International Conference on Neural Networks*, pp. 2403–2408, Perth, Australia, December 1995.

[25] X. Liu, Y. Wu, and B. Liu, "The research of adaptive sliding mode controller for motor servo system using fuzzy upper bound on disturbances," *International Journal of Control, Automation and Systems*, vol. 10, no. 5, pp. 1064–1069, 2012.

[26] Y. Wu, X. Liu, and D. Tian, "Research of compound controller for flight simulator with disturbance observer," *Chinese Journal of Aeronautics*, vol. 24, no. 5, pp. 613–621, 2011.

[27] H. S. LEE, *Robust digital tracking controllers for high-speed/high-accuracy positioning systems [Ph.D. thesis]*, University of California, Berkeley, Calif, USA, 1994.

[28] S. Yin, S. X. Ding, A. Haghani, H. Hao, and P. Zhang, "A comparison study of basic data-driven fault diagnosis and process monitoring methods on the benchmark Tennessee Eastman process," *Journal of Process Control*, vol. 22, no. 9, pp. 1567–1581, 2012.